Multiscale Energy Dissipation Mechanism in Tough and Self-Healing Hydrogels

Kunpeng Cui,[1] Tao Lin Sun,[1,2,3] Xiaobin Liang,[4] Ken Nakajima,[4] Ya Nan Ye,[5] Liang Chen,[5] Takayuki Kurokawa,[1,2] and Jian Ping Gong[1,2,6,*]

[1]*Faculty of Advanced Life Science, Hokkaido University, Sapporo 060-0810, Japan*
[2]*Soft Matter GI-CoRE, Hokkaido University, Sapporo 001-0021, Japan*
[3]*South China Advanced Institute for Soft Matter Science and Technology, South China University of Technology, Guangzhou 510640, China*
[4]*Department of Chemical Science and Engineering, Tokyo Institute of Technology, Tokyo 152-8552, Japan*
[5]*Graduate School of Life Science, Hokkaido University, Sapporo 060-0810, Japan*
[6]*Institute for Chemical Reaction Design and Discovery (WPI-ICRD), Hokkaido University, Sapporo 001-0021, Japan*

(Received 10 July 2018; revised manuscript received 28 September 2018; published 31 October 2018)

Understanding the energy dissipation mechanism during deformation is essential for the design and application of tough soft materials. We show that, in a class of tough and self-healing polyampholyte hydrogels, a bicontinuous network structure, consisting of a hard network and a soft network, is formed, independently of the chemical details of the hydrogels. Multiscale internal rupture processes, in which the double-network effect plays an important role, are found to be responsible for the large energy dissipation of these hydrogels.

DOI: 10.1103/PhysRevLett.121.185501

Hydrogels, composed of three-dimensional polymer networks and an abundance of water, tend to be brittle and weak, like fragile jellies [1]. Since 2000, spectacular progress has been achieved in creating mechanically strong and tough hydrogels even comparable to that of cartilages [2,3]. Toughening refers to the improvement in the fracture resistance of materials. The basic principle for toughening hydrogels is to introduce sacrificial bonds or energy dissipative structures [4–6], which categorize the developed gels into two groups. The first consists of double-network (DN) hydrogels with covalent bonds as sacrificial bonds [7,8]. This type of gel shows an elastic behavior and permanent softening after large deformation due to the irreversible nature of covalent bonds. The other group consists of supramolecular hydrogels with physical associations as sacrificial bonds [9–14]. This type of gel exhibits viscoelastic and self-healing behaviors from the reversible nature of physical associations.

From both fundamental and material application viewpoints, it is important to understand how energy dissipates in gels during deformation and failure processes. There has been progress in elastic DN gels and elastomers from both experimental [15–17] and theoretical aspects [18,19]. The internal breaking of covalent bonds in the first brittle network dissipates substantial amounts of energy and prevents macroscopic crack formation upon loading. While for viscoelastic supramolecular hydrogels, little is known on the structure and the energy dissipation mechanism. Because of the existence of physical associations, it is highly possible for those gels to arrange into different structures with different length scales.

In this Letter, we study strain-induced fracture in tough and self-healing supramolecular gels, focusing on the underlying energy dissipation mechanism and its relation to the structure. Supramolecular hydrogels composed of polyampholytes (PA) display viscoelasticity and excellent mechanical properties [10], such as high toughness, high fatigue resistance, and self-healing, making them perfect candidates for this study. By combining a customized extensional rheometer [20] and time-resolved synchrotron radiation small-angle x-ray scattering (SAXS), we elucidate that these PA gels have a multiscale structure and the toughening results from a synergistic effect involving multiscale energy dissipation.

PA gels were prepared by free radical copolymerization of oppositely charged monomers around charge balanced point in concentrated aqueous solution. Thereby on average the PA chains obtained carry the same amount of opposite charges randomly distributed on their backbones. After polymerization, the gels were dialyzed in water to remove the counterions, during which the ionic associations between opposite charges form and the gels shrink. In this work, we used two series of PA gels with different chemical structures (Fig. S1 and Table S1, in the Supplemental Material [21]). Hereafter, P(NaSS-*co*-MPTC) denotes the gels composed of ionic monomers sodium *p*-styrenesulphonate (NaSS) and 3-(methacryloylamino)propyl-trimethylammonium chloride (MPTC), P(NaSS-*co*-DMAEA-Q) for the gels composed of NaSS and methyl chloride quarternized *N*, *N*-dimethylamino ethylacrylate (DMAEA-Q), and the suffix -C_m-C_x after the name of copolymer denotes the total monomer concentration C_m (M) and chemical cross-linker

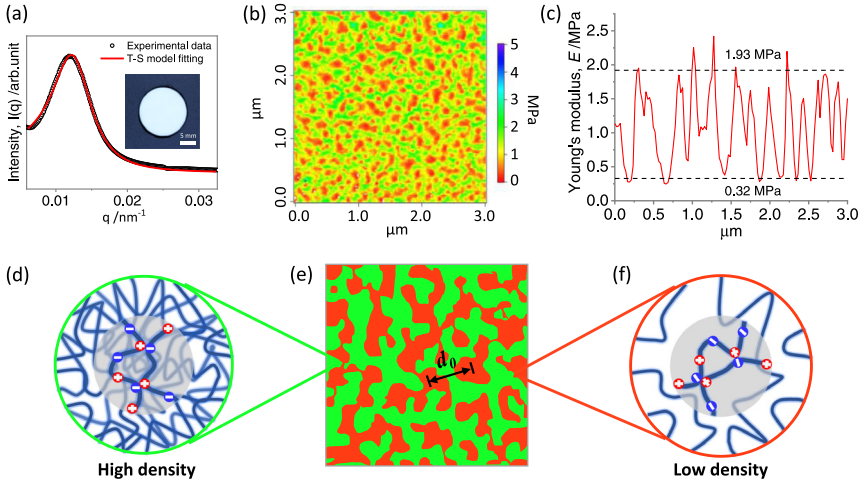

FIG. 1. Multiscale structure of polyampholytes (PA) hydrogels. (a) SAXS spectrum and Teubner-Strey (T-S) model fitting [23,24] for a PA hydrogel, P(NaSS-*co*-MPTC)-2.1-0, (b) 2D Young's modulus distribution obtained by nanomechanical mapping, and (c) a sectional profile. Inset in (a) shows an optical image of the gel. (d)–(f) Illustrations of the multiscale structure of PA gels: bicontinuous network structure consists of hard, dense regions (green) and soft, sparse regions (red) with a d_0 in hundred nanometers (e), aggregated polymer chains of dense (d) and sparse (f) regions at nanoscale, and ionic bonds at monomer scale [insets in (d) and (f)].

density C_x (mol %) relative to C_m. P(NaSS-*co*-MPTC) series have a higher softening temperature T_s (52 °C) than that of P(NaSS-co-DMAEA-Q) series (T_s around 20 °C). The former is much rigid (Young's modulus E: 2–3 MPa) than the latter (E: 0.06 MPa) at the observation temperature (24 °C). These gels, containing ~50 wt % of water, are highly stretchable and tough.

As an example, P(NaSS-*co*-MPTC)-2.1-0 gel is optically opaque [Fig. 1(a), inset], and exhibits a distinct peak in its SAXS spectrum [Fig. 1(a)]. AFM nanomechanical mapping [22] revealed a hundred nanometer scale structure consisting of irregular hard (green) and soft (red) regions [Fig. 1(b)]. The hard regions (~1.93 MPa) and the soft regions (~0.32 MPa) are similar in size and the spacing between adjacent hard (or soft) regions d_0 is about 500 nm [Fig. 1(c)]. AFM nanomechanical mapping on the stretched sample revealed that both the soft and hard regions were elongated along the stretching direction, showing the same anisotropy with that of the bulk sample (Fig. S2 [21]). This result indicates that the hard and soft regions form a bicontinuous structure. Accordingly, we used the Teubner-Strey model for a two-phase bicontinuous structure [23,24] to fit the SAXS peak [Fig. 1(a)], which also revealed a d_0 of 500 nm, in agreement with the results from AFM nanomechanical mapping. So the hard regions have higher polymer concentration than the soft regions, which gives contrast to the x ray. From these results, we revealed that the PA gels have a multiscale structure [Figs. 1(d)–1(f)]. At the monomer scale, the opposite charges associate to form ionic bonds; at the nanoscale, the charged chains aggregate into soft and hard regions; at the microscale, the soft and hard regions form a bicontinuous network; and at the macroscale, the gel is smooth and homogeneous.

Similar multiscale structure is observed for P(NaSS-*co*-DMAEA-Q) gels (Figs. S3, S4, and Table S1 in the Supplemental Material [21]). However, d_0 varies with the chemical structure of the PA gels. The P(NaSS-*co*-MPTC) series, having stronger ionic association, show larger d_0 (200–500 nm) in comparison with the P(NaSS-co-DMAEA-Q) series (72–155 nm). For the same monomer combination, d_0 becomes smaller with increasing monomer concentration or adding a chemical cross-linker in preparation (Table S1 [21]), suggesting that the decrease in the entanglement length or cross-linking length leads to small d_0. These results suggest that d_0 is determined by the competition between ion association-induced collapse of the PA chains and the resistance against the collapse due to cross-linking, where the topological entanglement and chemical cross-linking have similar effect on suppressing d_0.

To elucidate the energy dissipation mechanism and its relation to the multiscale structure, we performed time-resolved SAXS during tensile measurements using an extensional rheometer (Fig. S5a [21]). To have the structure change within the SAXS observation window, we first employed a P(NaSS-*co*-DMAEA-Q)-2.4-0.1 gel with $d_0 = 102$ nm.

A representative stress (σ)—stretch ratio (λ) curve and the corresponding 2D SAXS patterns are exhibited in Fig. 2(a). For low λ, the initial σ response is almost linear, followed by a softening around $\lambda = 1.5$, reflecting the breaking of ionic bonds [25,26]. The softening region continues up to quite high deformation ($\lambda = 5.0$), after which σ rises again, indicating the limiting chain extensibility effect [6]. The SAXS pattern shows an isotropic ring before deformation ($\lambda = 1.0$), demonstrating the isotropic distribution of soft and hard regions. Under stretch ($\lambda = 2.5$–5.0), the scattering ring

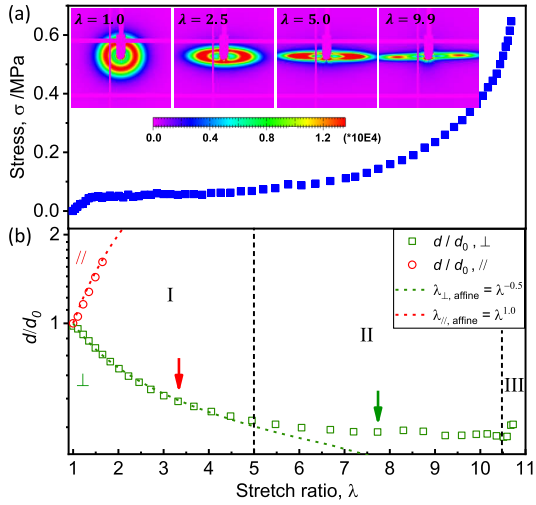

FIG. 2. Combined stress and structural measurements in a tensile test. (a) Nominal stress versus stretch ratio λ and the corresponding time-resolved 2D SAXS patterns at several representative λ. (b) Microscopic deformation ratio (d/d_0) in the parallel ($/\!/$) and perpendicular ($\perp$) directions of stretching versus λ. The dashed vertical lines mark the boundaries between three deformation regimes and the arrows indicate the two λ used in the recovery test of Fig. 3. Sample: P(NaSS-*co*-DMAEA-Q)-2.4-0.1 ($d_0 = 102$ nm). True strain rate: 0.05 s^{-1}. Stretching direction: vertical.

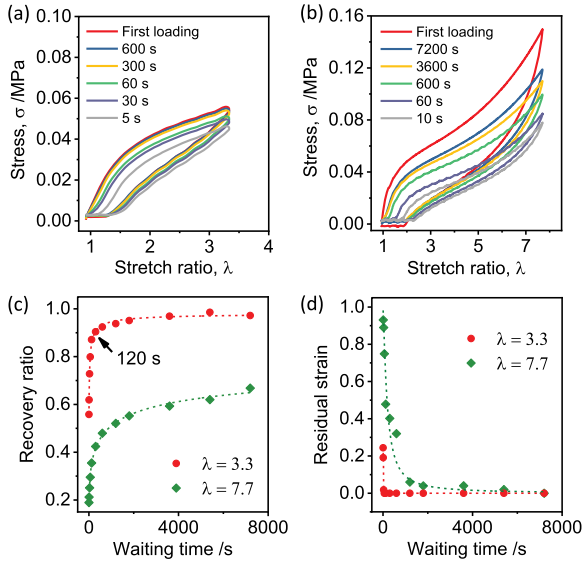

FIG. 3. Self-recovery behavior of gels under different deformations. (a),(b) Loading-unloading curves of the cyclic tensile test at different waiting times between the first and second cycles, for λ of 3.3 (a) and 7.7 (b). (c),(d) Waiting-time dependences of recovery ratio defined as the ratio of the second loading hysteresis loop to the first (c) and residual strain of sample after the first loading (d). Sample: P(NaSS-*co*-DMAEA-Q)-2.4-0.1 ($d_0 = 102$ nm).

converts into an ellipse with its major axis being perpendicular to the stretching direction, indicating that the d spacing increases in the stretching direction, while it decreases in the perpendicular direction. The scattering intensities concentrate within two elongated spots at very large deformation ($\lambda = 9.9$), suggesting the formation of highly anisotropic structures.

To quantify the time-resolved SAXS patterns and correlate them to the macroscopic mechanical behavior, we extract d spacing along the directions parallel ($d_{/\!/}$) and perpendicular ($d_\perp$) to the stretching based on the anisotropic nature of SAXS patterns (Fig. S5 [21]). From the d spacing at each deformation, we computed the d/d_0 for the microscopic deformation ratio of the bicontinuous network and correlated it with the macroscopic deformation ratio λ of the gels. Here d and d_0 are the d spacing at λ and at no deformation, respectively. As shown in Fig. 2(b), we observed three distinct regimes. Up to $\lambda = 5.0$, the microscopic deformations perfectly follow the affine deformations for an incompressible material [24,27], that is, $d_{/\!/}/d_0 = \lambda$ and $d_\perp/d_0 = \lambda^{-0.5}$. Above $\lambda = 5.0$, $d_\perp$ hardly decreases with increasing deformation over a large range (regime II, $\lambda = 5.0 - 10.5$). At very large deformation right before sample failure ($\lambda > 10.5$), $d_\perp$ increases again (regime III). We should mention that $d_{/\!/}$ is beyond the detection limit of SAXS from the middle of regime I.

To elucidate if there is any permanent structure damage during deformation, we performed a cyclic test on the gels. The gel was stretched to a preset deformation, followed by unloading at the same strain rate, and the second loading-unloading cycle was performed after a prescribed waiting time (Supplemental Material [21]). In regime I ($\lambda = 3.3$), the first loading-unloading curve has a large hysteresis, but the gels are rapidly (about 120 s) and fully recoverable [Figs. 3(a), 3(c), and 3(d)]. This strongly suggests that the large hysteresis in the affine deformation regime stems from energy dissipation due to breaking and reforming of ionic bonds at monomer scale and there is no permanent damage in the mesoscale bicontinuous networks. While in regime II ($\lambda = 7.7$), the large mechanical hysteresis remains even after a sufficiently long wait time [Figs. 3(b), 3(c)], but the sample fully shrinks back to its original size, showing no residual strain [Fig. 3(d)]. Those results indicate that permanent damage occurs in the hard network, but the soft network reverts to its original shape by its elasticity. This explains why in regime II, the sample shows nonaffine deformation. The bicontinuous structure prevents the catastrophic propagation of hard network rupture, leading to a large deformability of the materials before global failure.

From the above SAXS and self-recovery results, we discuss the structure change of the gel during deformation (Fig. 4). Up to a large $\lambda = \lambda_a = 5.0$, the deformation of the bicontinuous network is affine to the macroscopic deformation of gel (regime I). Here λ_a is the stretch ratio at the end of the affine deformation regime. In this regime, the two percolated networks deform equally, but the hard network

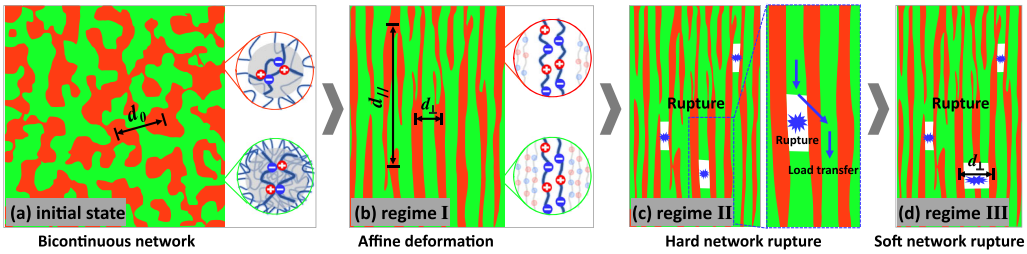

FIG. 4. Illustration of the multiscale fracture process of PA gels for high toughness. (a) The bicontinuous hard (green) and soft (red) networks with a length scale d_0 in the range of hundred nanometers were isotropic, and the polymer chains are in globule conformation due to ionic associations. (b) Under stretching, the ionic bonds break and the aggregated polymer chains unfold, permitting the bicontinuous network a very large reversible affine deformation. (c) With increasing deformation, some hard strands start to rupture, and the load is transferred to neighboring hard strands via soft strands. As the soft strands remain intact, the gel softens but still reverts to the original shape at unloading. (d) After rupture of most of the hard strands, the soft strands start to rupture, leading to global failure of the gel. Through such a multiscale rupture process, the gel dissipates a significant amount of energy, to show a high toughness.

sustains more stress due to high stiffness [Fig. 4(b)]. Such large affine deformation, which is rarely observed in other materials, is considered due to a synergy of two effects. The first is the globule chain conformation, as a consequence of ionic association [28,29]. It provides a large deformation capacity by transformation from globular into extended states under loading. The second is the stress redistribution mechanism originating from the bicontinuous structure. Although the bicontinuous network is statistically homogeneous, it contains some weak points along the contour of the strands that have a smaller cross section than average. The existence of soft strands allows gels to redistribute stress around weak points, thereby alleviating the stress concentrations and, consequently, allowing gels to show large affine deformation. Otherwise, during deformation the weak points would rupture easily due to the stress concentration.

In regime II, $d_\perp$ decreases slightly in a large deformation range, which could be understood by the rupture of the hard network [Fig. 4(c)]. At the end of affine deformation, the hard network is in a highly orientated state (Fig. S6 [21]), with the strands stretched along the direction parallel to the stretching, showing a large aspect ratio. Using the incompressible condition for hydrogels, the anisotropic ratio of strands is $d_{/\!/}/d_\perp = \lambda^{1.5}$, which reaches about 11 at the end of affine deformation ($\lambda_a = 5$). With further increasing deformation, the hard strands rupture as they carry most of the stress. The slight decrease in $d_\perp$ with the further increase in deformation in regime II suggests that the decrease in the d spacing by the transverse compression is cancelled by the rupture of hard strands that contract to release the stored elastic energy. The contraction of the ruptured hard strands exerts a large shear stress to the neighboring soft strands, as the hard and soft strands are connected by many bridged chains. The soft strands effectively transfer the shear stress to neighboring unruptured hard strands [Fig. 4(c)]. With the increase of λ in regime II, more hard strands are ruptured. Once the shear stress is larger than the strength of soft strands, the soft strands rupture [Fig. 4(d)], which destroys the ordering with the neighboring hard strands, leading to a significant increase in $d_\perp$ [Fig. 2(b)]. This explains what happened in regime III. For some gels, the spotlike scattering transforms into streaklike scattering in the SAXS pattern near gel fracture (Fig. S7 [21]), suggesting that the structure correlation between strands disappears due to the rupture of significant amounts of soft strands or generation of large-scale heterogeneity.

From the explanation that the decrease in the d spacing by the transverse compression is cancelled by the rupture of hard strands, we can quantitatively estimate the fraction of ruptured hard strands along the stretch direction in regime II, $r_{\rm rap}$, from the relation $r_{\rm rap} = 1 - \lambda_a/\lambda$ (Supplemental Material [21]). At the end of regime II, $\lambda = 10.5$ from Fig. 2(b), we found that about half of the hard strands are ruptured. Further increase in deformation leads to the rupture of the soft strands and the global failure of the material.

To elucidate if such a multiscale fracture process is generic for other PA hydrogels, we studied the structure change during stretching for other samples, the soft P(NaSS-*co*-DMAEA-Q)-2.8-0.1 gels with a smaller $d_0 =$ 72 nm and two rigid P(NaSS-*co*-MPTC) gels with large d_0 of 200 (P(NaSS-*co*-MPTC)-2.1-0.1) and 500 nm (P(NaSS-*co*-MPTC)-2.1-0) (Table S1 [21]). These samples also exhibit large affine and extensive nonaffine deformation regimes in the studied strain rates (Fig. S8 [21]). We found that the rigid P(NaSS-*co*-MPTC)-2.1-0 gels also show fully self-recovery in affine deformation regime and partial recovery of stress in nonaffine deformation regime but with no residual strain (Fig. S9 [21]). These behaviors are similar to that of the soft P(NaSS-*co*-DMAEA-Q)-2.4-0.1 gels (Fig. 3), although it took much longer for the rigid P(NaSS-*co*-MPTC)-2.1-0 gels to recovery. Therefore, only the relative strength of the rigid and soft networks, but not their absolute values, is relevant for the multiscale fracture process. These results confirm the universal nature of the structure evolution and energy dissipation mechanism of PA gels under deformation, independent of the sample stiffness and relaxation dynamics.

The stress-transferring and crack-stopping mechanisms observed in the PA gels possess some similarities to the tough DN gels, which consist of an interpenetrated rigid (brittle) network and a soft (stretchy) network with a mesh size of ∼10 nm. The first network ruptures first upon loading, transferring the stress to the second network that holds the microcrack and disperses the stress to a large area, leading to the high toughness of DN gels.

To conclude, our study highlights the role of multiscale structures on energy dissipation of tough and self-healing supramolecular hydrogels. The hierarchical structure endows gels with a multiscale fracture process. With increasing deformation, first the breaking of the ionic bonds in monomer scale occurs to induce unfolding of the globule chains (regime I); then the rupture of hard strands in a mesoscale bicontinuous network structure occurs while the soft strands effectively disperse the stress, preventing the catastrophic crack propagation (regime II); finally, the soft strands also rupture, leading to catastrophic fracture of the sample (regime III). Such a multiscale rupture process dissipates a significant amount of energy, contributing to the high toughness of the soft materials. We consider that a similar multiscale energy dissipation mechanism might account for the toughening of some phase-separated systems, such as toughening of polyacrylamide gels in poor solvent [30] and toughening of thermoresponsive poly(*N*-isopropylacrylamide)-based gels at high temperature [24]. The high toughness observed in amorphous polymers around their glass transition regime might also be related to a similar mechanism due to formation of dynamical heterogeneities [31].

We thank Wei Hong for helpful discussion and Liangbin Li for providing extensional rheometers. The SAXS experiments were performed at NCPSS BL19U2 beam line at SSRF, China and USAXS experiments at BL20XU beam line at Spring-8, Japan. This research was supported by JSPS KAKENHI (Grant No. JP17H06144), and by ImPACT Program of Council for Science, Technology and Innovation (Cabinet Office, Government of Japan). The Institute for Chemical Reaction Design and Discovery (ICRD) was established by World Premier International Research Initiative (WPI), MEXT, Japan.

*Corresponding author.
gong@sci.hokudai.ac.jp

[1] F. Ullah, M. B. H. Othman, F. Javed, Z. Ahmad, and H. M. Akil, Mater. Sci. Eng. C **57**, 414 (2015).
[2] J. P. Gong, Science **344**, 161 (2014).
[3] Y. S. Zhang and A. Khademhosseini, Science **356**, eaaf3627 (2017).
[4] J. P. Gong, Soft Matter **6**, 2583 (2010).
[5] X. Zhao, Soft Matter **10**, 672 (2014).
[6] C. Creton, Macromolecules **50**, 8297 (2017).
[7] J. P. Gong, Y. Katsuyama, T. Kurokawa, and Y. Osada, Adv. Mater. **15**, 1155 (2003).
[8] R. E. Webber, C. Creton, H. R. Brown, and J. P. Gong, Macromolecules **40**, 2919 (2007).
[9] J.-Y. Sun, X. Zhao, W. R. K. Illeperuma, O. Chaudhuri, K. H. Oh, D. J. Mooney, J. J. Vlassak, and Z. Suo, Nature (London) **489**, 133 (2012).
[10] T. L. Sun, T. Kurokawa, S. Kuroda, A. Bin Ihsan, T. Akasaki, K. Sato, T. Nakajima, J. P. Gong, M. A. Haque, T. Nakajima, J. P. Gong, and M. A. Haque, Nat. Mater. **12**, 932 (2013).
[11] J. Brassinne, A. Cadix, J. Wilson, and E. van Ruymbeke, J. Rheol. **61**, 1123 (2017).
[12] J. He, S. Aktas, S. A. Sukhishvili, and D. M. Kalyon, J. Rheol. **61**, 1135 (2017).
[13] J. Zhao, K. Mayumi, C. Creton, and T. Narita, J. Rheol. **61**, 1371 (2017).
[14] M. A. Gonzalez, J. R. Simon, A. Ghoorchian, Z. Scholl, S. Lin, M. Rubinstein, P. Marszalek, A. Chilkoti, G. P. López, and X. Zhao, Adv. Mater. **29**, 1604743 (2017).
[15] Q. M. Yu, Y. Tanaka, H. Furukawa, T. Kurokawa, and J. P. Gong, Macromolecules **42**, 3852 (2009).
[16] Y. Tanaka, Y. Kawauchi, T. Kurokawa, H. Furukawa, T. Okajima, and J. P. Gong, Macromol. Rapid Commun. **29**, 1514 (2008).
[17] E. Ducrot, Y. Chen, M. Bulters, R. P. Sijbesma, and C. Creton, Science **344**, 186 (2014).
[18] H. R. Brown, Macromolecules **40**, 3815 (2007).
[19] X. Wang and W. Hong, Soft Matter **7**, 8576 (2011).
[20] Y. Liu, W. Zhou, K. Cui, N. Tian, X. Wang, L. Liu, L. Li, and Y. Zhou, Rev. Sci. Instrum. **82**, 045104 (2011).
[21] See Supplemental Material at http://link.aps.org/supplemental/10.1103/PhysRevLett.121.185501 for the sample details, the experimental and data analysis methods, the method to calculate the fraction of ruptured hard strands, a SAXS pattern for gel before rupture, the orientation of bicontinuous network, the universal nature of the structure evolution of gels during deformation, and the self-recovery behavior of P(NaSS-co-MPTC)-2.1-0 gels under different strain.
[22] D. Wang, X. Liang, T. P. Russell, and K. Nakajima, Macromolecules **47**, 3761 (2014).
[23] M. Teubner and R. Strey, J. Chem. Phys. **87**, 3195 (1987).
[24] H. Guo, N. Sanson, D. Hourdet, and A. Marcellan, Adv. Mater. **28**, 5857 (2016).
[25] T. L. Sun, F. Luo, W. Hong, K. Cui, Y. Huang, H. J. Zhang, D. R. King, T. Kurokawa, T. Nakajima, and J. P. Gong, Macromolecules **50**, 2923 (2017).
[26] K. Cui, T. L. Sun, T. Kurokawa, T. Nakajima, T. Nonoyama, L. Chen, and J. P. Gong, Soft Matter **12**, 8833 (2016).
[27] Q. Wen, A. Basu, P. A. Janmey, and A. G. Yodh, Soft Matter **8**, 8039 (2012).
[28] A. V. Dobrynin, R. H. Colby, and M. Rubinstein, J. Polym. Sci. B **42**, 3513 (2004).
[29] G. Nisato, J. P. Munch, and S. J. Candau, Langmuir **15**, 4236 (1999).
[30] K. Sato, T. Nakajima, T. Hisamatsu, T. Nonoyama, T. Kurokawa, and J. P. Gong, Adv. Mater. **27**, 6990 (2015).
[31] R. J. Masurel, P. Gelineau, S. Cantournet, A. Dequidt, D. R. Long, F. Lequeux, and H. Montes, Phys. Rev. Lett. **118**, 047801 (2017).